RSC Advances

PAPER

View Article Online
View Journal | View Issue

Cite this: *RSC Adv.*, 2023, **13**, 14210

The solvent effect on the morphology and molecular ordering of benzothiadiazole-based small molecule for inkjet-printed thin-film transistors †

Cuc Kim Trinh, *[ab] Ha Som Oh[c] and Hanleem Lee*[cd]

Received 29th March 2023
Accepted 29th April 2023

DOI: 10.1039/d3ra02036c

rsc.li/rsc-advances

A small molecule organic semiconductor, D(D′–A–D′)$_2$ comprising benzothiadiazole as an acceptor, 3-hexylthiophene, and thiophene as donors, was successfully synthesized. X-ray diffraction and atomic force microscopy were used to investigate the effect of a dual solvent system with varying ratios of chloroform and toluene on film crystallinity and film morphology *via* inkjet printing. The film prepared with a chloroform to toluene ratio of 1.5 : 1 showed better performance with improved crystallinity and morphology due to having enough time to control the arrangement of molecules. In addition, by optimizing ratios of $CHCl_3$ to toluene, the inkjet-printed TFT based on **3HTBTT** using a $CHCl_3$ and toluene ratio of 1.5 : 1 was successfully fabricated and exhibited a hole mobility of 0.01 $cm^2 V^{-1} s^{-1}$ due to the improved molecular ordering of the **3HTBTT** film.

Introduction

Over the past few decades, inkjet printing techniques have been widely employed for the fabrication of various thin-film devices, such as field-effect transistors (OTFTs),[1–5] light-emitting diodes (LEDs),[6,7] solar cells,[8–11] sensors,[12–14] *etc.* These inkjet printing methods have garnered significant attention due to their potential benefits such as ultra-low-cost, non-vacuum, and environmentally friendly processability.[1,15] Compared to the spin-coating technique, using inkjet techniques can minimize the waste of materials and simplify the manufacturing process. Furthermore, the materials are deposited *via* a solution process under mild conditions (*i.e.*, room temperature, no vacuum assistance) during the inkjet printing process. This allows easy fabrication of flexible electronics on large-area substrates.[16–18] Printed electronics can be applied to flexible substrates such as plastic, paper, and fabric, making them suitable for use in wearable devices, smart textiles, and other applications where flexibility is required. Furthermore, they can be easily integrated with other electronic components, such as sensors and batteries, facilitating the development of more complex systems and devices.

Conjugated polymers and small-molecules organic semiconductors have proven to be extremely effective materials in the development of printable electronic devices.[19–26] There has been a growing interest in the small molecules-based optoelectronic application in recent years. Small molecules offer several advantages over polymer-based organic electronics, such as a well-defined chemical structure, molecular structure, and high purity, making them easy to reproduce.[27–29] High-performance small molecule-based organic semiconductors are widely used in inkjet-printing devices due to their low-temperature processability and good solubility in various organic solvents, which are important advantages of the inkjet printing process.

Despite their potential benefits, there are numerous challenges that must be overcome in the development of p-type organic semiconductors to enable their widespread use in electronic devices. One of the key challenges is the attainment of high carrier mobility. Although significant advancements have been made in recent years, the mobility of p-type organic semiconductors generally remains lower than that of n-type organic semiconductors, which can restrict the overall performance and efficiency of devices employing p-type semiconductors. Another significant obstacle is the achievement of high stability and reliability of p-type organic semiconductors, particularly in harsh environments or over extended periods of use. Nevertheless, to realize flexible printed electronics, it is crucial to develop stable and durable p-type organic

[a]*Chemical Engineering in Advanced Materials and Renewable Energy Research Group, School of Technology, Van Lang University, Ho Chi Minh City, Vietnam. E-mail: cuc.tk@vlu.edu.vn*

[b]*Faculty of Applied Technology, School of Technology, Van Lang University, Ho Chi Minh City, Vietnam*

[c]*Department of Chemistry, Myongji University, 116 Myongji Ro, Yongin, Gyeonggi-do, Republic of Korea. E-mail: hanleem@mju.ac.kr*

[d]*The Natural Science Research Institute, Myongji University, 116 Myongji Ro, Yongin, Gyeonggi-do, South Korea*

† Electronic supplementary information (ESI) available. See DOI: https://doi.org/10.1039/d3ra02036c

semiconductors. Moreover, printed TFTs are exposed to considerable quantities of H_2O and O_2 during the manufacturing process, which can exacerbate degradation during operation. Enhancing the molecular assembly between molecules can help minimize the capture of H_2O and O_2 in the channel, which can improve operational stability. Especially, the presence of insulating solubilizing groups, such as alkyl side chains, can hinder charge transport between molecules and affect the morphology of self-assembled films, thereby reducing intermolecular interaction. Hence, it is important to control the position of side chains on the molecular structure to avoid the twisted core and reduce π-conjugation. To address these issues, many researchers have investigated various small molecules with highly ordered structures and strong intermolecular interaction by controlling the ordering of the molecules, thereby enhancing the charge transport between them.[30–34] By controlling the size and position of the alkyl chains and utilizing donor or acceptor moieties with high planarity and strong intermolecular interaction, molecular ordering between molecules can be improved.

In the present investigation, we have developed novel organic semiconductors, D(D′–A–D′)$_2$, comprising benzothiadiazole (BT) as the acceptor (A) unit and 3-hexylthiophene (3HT) as the second donor (D′), to leverage the improved intermolecular interactions arising from the planar 3HT–BT–3HT structure.[35–37] The attachment of hexyl chains to the fourth positions in the thiophene rings (from the central BT moiety) has facilitated solubility enhancement and avoided steric hindrance from insulating alkyl chains.[35,38] Furthermore, the thiophene moiety as the donor unit in the middle of the system has played a pivotal role in boosting the π–π conjugated system, without compromising the planarity of the entire system. Finally, a new organic semiconductor material was successfully synthesized. In addition, we studied the effect of a dual solvent system with varying ratios of chloroform and toluene on the film morphology. A single solvent system, such as chlorobenzene, chloroform, or toluene, has demonstrated poor film morphologies and low crystallinity, resulting in extremely low carrier mobility in organic electronic devices.[39–41] However, by modulating the ratios of $CHCl_3$ to toluene, inkjet-printed TFT devices' electrical properties and uniformity have been substantially improved.

Experimental

General instruments and measurements

The small molecule was characterized by ^{1}H and ^{13}C NMR spectroscopy using a JEOL JNM-LA 400 FT-NMR at 25 °C. Differential scanning calorimetry (DSC) was performed on a TA instrument (DSC-TA Q-20 Instrument) at a 10 °C min^{-1} heating rate under N_2. The absorptions of the small molecule, both in solution and as a film, were measured using a UV-vis spectrophotometer (Varian, Cary 5000). To prepare the film samples, 10 mg of a small molecule was dissolved in 1 ml of chloroform, and the film samples were prepared by spin-coating on a glass substrate. The molecular ordering and crystallinity of the thin films were confirmed by X-ray diffractometry using a Rigaku D/max-2500 diffractometer with Cu K_α radiation ($\lambda = 1.5418$ Å) at 40 kV and 100 mA. The surface roughness of the thin films was evaluated using an atomic force microscope (PSIA, XE-200).

Materials and synthesis

2,5-Bis(tributylstannyl)thiophene (97%), tetrakis(triphenylphosphine) palladium(0) ($Pd(PPh_3)_4$, 99%), *n*-bromosuccinimide (NBS, 99%), tetrahydrofuran (anhydrous, 99.9%), toluene (anhydrous, 99.8%) were purchased from Sigma-Aldrich company. 4,7-Dibromo-2,1,3-benzothiadiazole (98%), 4-hexyl-2-(4,4,5,5-tetramethyl-1,3,2-dioxaborolan-2-yl)thiophene (98%) were purchased from TCI company. All chemicals were used without further purification. 4,7-Bis(4-hexylthiophen-2-yl)benzo[*c*][1,2,5] thiazole (**1**) was prepared according to a previously published procedure.[35]

Synthesis of 4-(5-bromo-4-hexylthiophen-2-yl)-7-(4-hexylthiophen-2-yl)benzo[*c*][1,2,5] thiadiazole (2). A solution of 4,7-bis(4-hexylthiophen-2-yl)benzo[*c*][1,2,5] thiazole (**1**) (0.5 g, 1.07 mmol) in 12 ml of anhydrous THF was prepared in a 2-neck-flask. The mixture was degassed for 30 minutes and then *n*-bromosuccinimide (NBS) (0.21 mg, 1.17 mmol) dissolved in 10 ml of anhydrous THF was added dropwise over 30 minutes at 0 °C. The reaction was protected from light during the addition and stirred for an additional 30 minutes at 0 °C and 30 minutes at room temperature. The reaction mixture was then extracted with ethyl acetate and DI water, and the organic layer was dried over anhydrous Na_2SO_4 overnight. The solvent was removed by evaporation and the product was purified by column chromatography using hexane as the eluent. The yield was 72% (0.4 g) and the product was obtained as an orange solid. ^{1}H NMR (400 MHz, $CDCl_3$), δ (ppm): 7.98 (s, 1H), 7.81 (d, 1H), 7.76 (d, 1H), 7.35 (s, 1H), 7.04 (s, 1H), 2.70–2.61 (t, 4H), 1.69 (m, 4H), 1.51–1.27 (m, 12H), 0.88–0.86 (t, 6H). ^{13}C NMR (100 MHz, $CDCl_3$), δ (ppm): 152.6, 144.5, 143.1, 138.9, 138.7, 129.3, 126.4, 125.4, 125.0, 121.8, 111.4, 31.7, 30.7, 29.8, 29.1, 22.7, 14.2.

Synthesis of 7,7′-(3,3″-dihexyl-[2,2′:5′,2″-terthiophene]-5,5″-diyl) bis(4-(4-hexylthiophen-2-yl)benzo[*c*][1,2,5]thiadiazole) (3HTBTT). Compound **2** (137 mg, 0.25 mmol), 2,5-bis(tributylstannyl)-thiophene (100 mg, 0.1 mmol), and $Pd(PPh_3)_4$ (13.8 mg, 0.012 mmol) were dissolved in 15 ml of anhydrous toluene and degassed with nitrogen for 30 min before refluxing at 90 °C for 7 h under an argon atmosphere. The reaction mixture was extracted with dichloromethane and DI-water and dried over anhydrous Na_2SO_4. The solvent was removed by evaporation, and the product was purified by column chromatography (hexane: CH_2Cl_2) to afford a dark purple solid (68 mg, yield: 68%). ^{1}H NMR (400 MHz, $CDCl_3$), δ (ppm): 8.02–8.01 (d, 4H), 7.86 (s, 2H), 7.28 (s, 4H), 7.05 (s, 2H), 2.74–2.71 (t, 8H), 1.81 (m, 8H), 1.53–1.28 (m, 24H), 0.95–0.92 (t, 12H). ^{13}C NMR (100 MHz, $CDCl_3$), δ (ppm): 153.1, 144.7, 140.6, 139.0, 137.0, 131.9, 130.9, 129.0, 126.3, 125.1, 125.3, 121.0, 32.2, 30.4, 29.7, 29.2, 22.4, 13.8. Anal. calcd for $C_{56}H_{64}N_4S_7$ (%): C, 66.10; H, 6.34; N, 5.51. Found: C, 66.05; H, 6.32; N, 5.48.

Devices fabrication and characterization of inkjet printing TFT

The hole-only device was fabricated by the following process. Patterned glass/ITO substrates (with a sheet resistance of 20 Ω

per in.^{2}) were procured commercially and subjected to a rigorous cleaning process involving sonication in water, acetone, and isopropyl alcohol (IPA) for a duration of 10 minutes. The cleaned substrates were then treated with O_2 plasma for 1 minute at a power of 50 W. A uniform layer of PEDOT: PSS (Baytron AI4083) with a thickness of 50 nm was subsequently deposited on the ITO glass surface using a spin-coating process. The organic film was then formed on the PEDOT: PSS layer using inkjet printing. Finally, a shadow mask was utilized to deposit a 10 nm-thick layer of MoO_3 and a 100 nm-thick layer of Ag electrode through thermal vacuum evaporation. The hole-only devices were structured as ITO/PEDOT: PSS/organic film/MoO_3/Ag.

The TFT device was fabricated on a pre-patterned FET device that was designed on a p-doped Si gate substrate with a SiO_2 layer of 300 nm thickness. The top source/drain electrodes, consisting of chromium (Cr) (5 nm) and gold (Au) (80 nm), were separated by varying channel distances of 20 to 150 μm. Semiconductor material was inkjet printed on the pre-patterned FET devices using different solvent systems. The film was subsequently dried in an 80 °C oven for 60 minutes. Each transfer and output curve was measured using a Keithley 4200 semiconductor characterization system at room temperature and under a vacuum pressure of 10^{-4} to 10^{-5} Torr. Mobility was calculated by

$$g_m = \frac{\partial I_{DS}}{\partial V_{GS}}\bigg|_{V_{DS}} = \mu C_{ox}\frac{W}{L}V_{DS}$$

Results and discussion

Synthesis and characterization of 3HTBTT small molecules

Compound **2** was prepared by reacting 4,7-bis(4-hexylthiophen-2-yl)benzo[*c*][1,2,5] thiazole (**1**) with *n*-bromosuccinimide in anhydrous THF. Subsequently, 7,7′-(3,3″-dihexyl-[2,2′:5′,2″-terthiophene]-5,5″-diyl)bis(4-(4-hexylthiophen-2-yl)benzo[*c*][1,2,5]-thiadiazole) small molecule (**3HTBTT**) was synthesized *via* stille coupling reaction of compound **2** and 2,5-bis(tributylstannyl) thiophene in the presence of Pd catalyst. The yield of the reaction was approximately 68%, as determined by NMR and elementary analysis (Scheme 1). The ^{1}H NMR and ^{13}C NMR of **3HTBTT** are presented in ESI Fig. S2.† Due to the presence of two thiadiazole units, the chemical shift of this carbon nucleus (δ = 129.0 ppm) in the final product is likely shifted downfield compared to the corresponding carbon in compound **2**. This is due to the electron-withdrawing effect of the thiadiazole rings. As we expected, the solubility of the final product in common organic solvents such as chloroform and THF was excellent due to the four hexyl chains. The self-assembly ability of the synthesized **3HTBTT** was further evaluated using differential scanning calorimetry (DSC), which showed a glass temperature (T_g) of 94.9 °C (Fig. 1). The glass transition temperature (T_g) indicates the temperature at which a material undergoes a transition from a rigid, glassy state to a more flexible, rubbery state or *vice versa*, signifying a crucial point in the formation of amorphous glass. The relatively high T_g value of the material

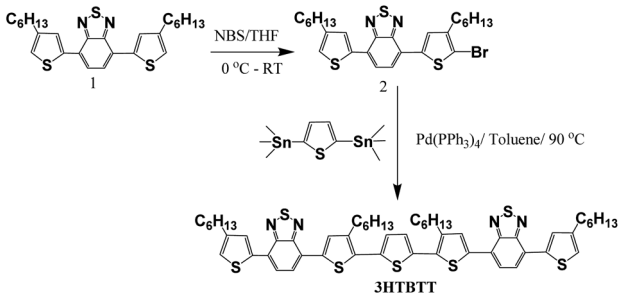

Scheme 1 Synthesis route for **3HTBTT** small molecule.

was attributed to non-covalent S···N interaction, indicating the ease of manipulating molecular alignment of **3HTBTT** through well-organized structures and strong intermolecular interactions between molecules.[42–46]

Optical properties

The UV-vis absorption spectra of **3HTBTT** small molecule were shown in Fig. 2. The onset wavelength in the solid state (λ_{onset} = 709.4 nm) was red-shifted by approximately 100 nm compared to that of **3HTBTT** in solution (λ_{onset} = 604.7 nm) due to the improved molecular ordering between molecules and improved π-stacking in the solid state.[47–49] The optical band gap of the small molecule was also reduced from 2.05 eV in the solution to 1.75 eV in the film, which is consistent with the trend of λ_{onset}. All λ_{max}, λ_{onset}, and optical band gaps (E_g^{op}) are summarized in Table 1.

Film properties

To investigate the crystallinity, molecular ordering, and solvent effect on the morphology film before and after patterning with different ratios of $CHCl_3$: toluene, XRD measurements were carried out (Fig. 3 and 4). The material was dissolved in different ratios of $CHCl_3$: toluene, such as 0 : 1, 1 : 1, 1.5 : 1, and 2 : 1. The solvent plays a critical role in controlling the arrangement of molecules in the film.[40,50] The fluidic dynamics

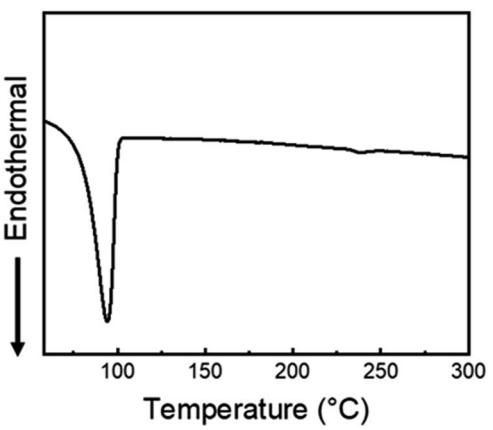

Fig. 1 Differential scanning calorimetry (DSC) curve of **3HTBTT** small molecule. The DSC showed a clear melting peak.

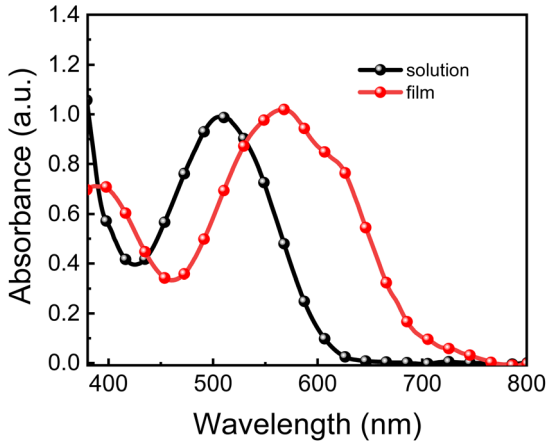

Fig. 2 UV absorption spectra of **3HTBTT** small molecule in $CHCl_3$ (black line) and solid-state film (red line).

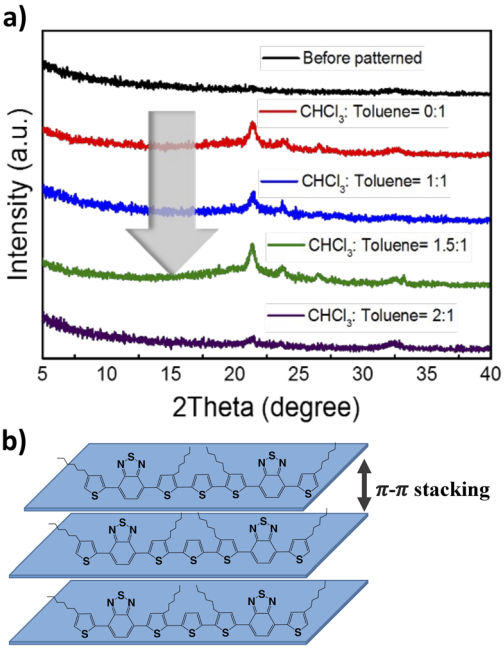

Fig. 3 (a) XRD spectra of random **3HTBTT** film (black line) and **3HTBTT** film *via* inkjet printing with different ratios $CHCl_3$: toluene. (b) Schematic illustration of proposed **3HTBTT** molecular arrangement after applying inkjet printing technique.

in chloroform and toluene differ due to their influence on the ink's evaporation and convection behavior. Although the material readily dissolves in chloroform, its low boiling point of 61.15 °C, evaporation rate of 29.4 kJ mol^{-1}, and combustion enthalpy of −473.21 kJ mol^{-1} impede the proper organization of the molecules during the drying process. In contrast, toluene higher boiling point of 110.6 °C, an evaporation rate of 38.064 kJ mol^{-1}, and a combustion enthalpy of −3910.3 kJ mol^{-1}. Therefore, a co-solvent system using $CHCl_3$ and toluene effectively modulates the ink's fluidic dynamics without compromising the solubility of small molecules. Specific ratios of the co-solvent system provide the film with enough time to control the arrangement of molecules, resulting in enhanced crystallinity and morphology, as shown in Fig. 3 and 4.

To provide a comprehensive comparison, a sample of randomly oriented **3HTBTT** was fabricated using a spin-coating technique with a high boiling point solvent, but without heat treatment. However, due to the relatively low intermolecular interaction between the π–π orbitals of the small molecule compared to the polymer, the resulting film exhibited minimal self-assembly, and consequently, no diffraction peaks associated with the π–π intermolecular interaction between the molecules were observed. In contrast, the application of the inkjet printing technique resulted in the emergence of new peaks at $2\theta = 21.38°$ corresponding to a *d*-spacing of 0.42 nm, as illustrated in Fig. 3. These peaks were attributed to the π–π stacking between the conjugated chains.[45,46] It is postulated that the strong intermolecular interaction between the molecules was facilitated through solvent engineering during the inkjet process, improving the crystallinity of the films. The chemical arrangement of **3HTBTT** after applying the inkjet printing technique is proposed as shown in Fig. 3b.

An increase in the volume of $CHCl_3$ in the solvent mixture ($CHCl_3$ and toluene) resulted in a stronger intensity of the diffraction peak related to π–π stacking, particularly when the ratio of $CHCl_3$ to toluene was 1.5 : 1. This phenomenon can be attributed to the polarity of chloroform relative to toluene. However, as the ratio of chloroform was increased up to 2 : 1 compared to the volume of toluene, the peak associated with π–π stacking was observed to decrease. This was likely due to the rapid evaporation of the ink, which hindered the effective modulation of intermolecular interaction. Furthermore, the film morphology of inkjet-printed **3HTBTT** on ITO substrate

Table 1 Optical properties of **3HTBTT** small molecules

UV-vis absorption						
	Solution[a]			Film		
Material	λ_{max} (nm)	λ_{onset} (nm)	E_g^{op} [b] (eV)	λ_{max} (nm)	λ_{onset} (nm)	E_g^{op} [b] (eV)
3HTBTT	508.4	604.7	2.05	568.7	709.4	1.75

[a] Samples were prepared from chloroform solution. [b] Optical band gap E_g^{opt} was calculated from using the onset of the UV-vis spectrum ($E_g^{opt} = 1240/\lambda_{onset}$).

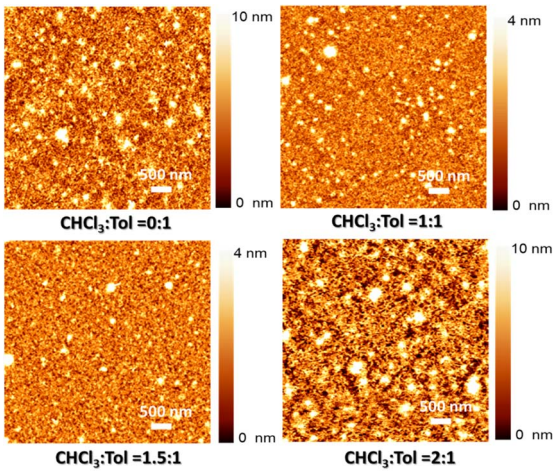

Fig. 4 AFM images of **3HTBTT** film *via* inkjet printing with different ratios $CHCl_3$: toluene.

exhibited varying surface roughness depending on the ratio of $CHCl_3$ to toluene (as shown in Fig. 4). The obtained surface roughness values were found to be 6.38 nm, 1.81 nm, 1.05 nm, and 10.02 nm for $CHCl_3$ to toluene ratios of 0 : 1, 1 : 1, 1.5 : 1, and 2 : 1, respectively. It was observed that the XRD data showed a remarkable agreement with the AFM data, indicating a significant reduction in both aggregation and surface roughness of the thin films as the volume concentration of chloroform in the mixture was increased up to a ratio of 1.5 : 1. However, beyond this ratio, the thin film with the highest ratio of chloroform in the mixture exhibited the highest surface roughness. This confirms that the solvent mixture with the appropriate concentration induced the fine assembly of small molecules, thereby enhancing charge transport and ultimately leading to improved device performance.

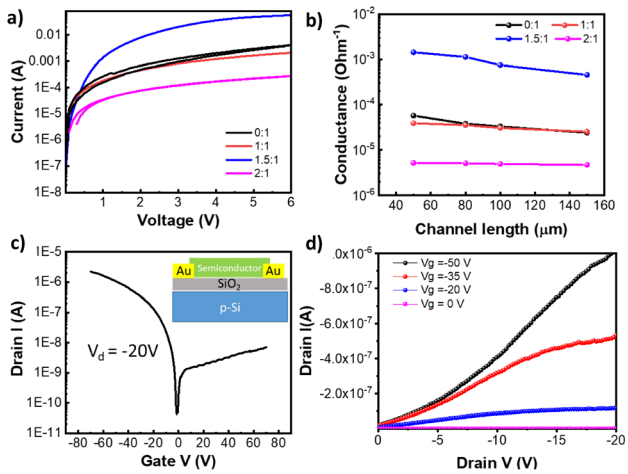

Fig. 5 (a) *I*–*V* curve for HOD devices with different ratios $CHCl_3$: toluene. (b) Conductance *versus* channel length plots with different ratios $CHCl_3$: toluene. (c) Transfer curve and (d) output curve for printed TFT device with 1.5 : 1 solution.

Electrical properties of 3HTBTT film

To accurately evaluate the charge carrier transportation characteristics of molecular-scale ordered **3HTBTT** films with varying ratios of $CHCl_3$ and toluene, the hole mobility of each material was meticulously extracted from the corresponding hole-only device. To account for the asymmetry of the Fermi level in the PEDOT: PSS and MoO_3 layers, a precisely calibrated built-in internal field of approximately 0.39 V was generated, thus ensuring that the measured *J*–*V* characteristics were accurately corrected by the corresponding built-in potential. Subsequently, the space-charge-limited conduction (SCLC) region was fitted using the Mott–Gurney law, including the built-in voltage ($V_{built\text{-}in}$) correction term, expressed as

$$J = \frac{9}{8}\mu\varepsilon_s \frac{(V - V_{built\text{-}in})^2}{L^3}$$

where μ is the charge carrier mobility, ε_s is the permittivity of the materials, and L is the thickness of the film. Assuming a dielectric constant of 3, the calculated hole mobility of **3HTBTT** was found to be 1.5×10^{-5} cm^2 V^{-1} s^{-1}, 5.9×10^{-4} cm^2 V^{-1} s^{-1}, 9.5×10^{-4} cm^2 V^{-1} s^{-1}, and 1.6×10^{-6} cm^2 V^{-1} s^{-1}, for $CHCl_3$ to toluene ratios of 0 : 1, 1 : 1, 1.5 : 1, and 2 : 1, respectively (Fig. 5a). We conducted additional measurements of our materials' conductivity to observe the intrinsic properties of the films. The observed conductivity values were 1.60 S cm^{-1}, 1.45 S cm^{-1}, 38 S cm^{-1}, 0.23 S cm^{-1} for $CHCl_3$ to toluene ratios of 0 : 1, 1 : 1, 1.5 : 1, and 2 : 1, respectively (Fig. 5b). As previously mentioned, the enhanced mobility and conductivity were attributed to the successful formation of a highly ordered **3HTBTT** film using a $CHCl_3$ and toluene ratio of 1.5 : 1. Finally, we successfully fabricated inkjet-printed TFTs using **3HTBTT** small molecule with the optimized solvent system (*i.e.*, $CHCl_3$ to toluene ratio of 1.5 : 1). The transfer curve (Fig. 5c) and output curve (Fig. 5d) of **3HTBTT** indicated relatively high hole mobility of approximately 0.01 cm^2 V^{-1} s^{-1} (transconductance = 0.024 μS) with a high on/off ratio (=10^4), even without post-annealing. Although the mobility was still lower than desired due to the high number of interface defects under the pre-fabricated FET device structure, we believe that this value demonstrated quite a high performance among other small molecule-based inkjet printed TFTs published to date.

Conclusions

We successfully synthesized **3HTBTT** small molecule with D(D′–A–D′)$_2$ structure system. Various ratios of $CHCl_3$: toluene used to control the morphology film and molecular arrangement *via* inkjet printing technology were studied by XRD and AFM. The results clearly showed that the morphology film and their crystallinity were dramatically enhanced with suitable ratios of $CHCl_3$: toluene. This resulted in a significant improvement in charge carrier transport. The mobilities estimated from **3HTBTT**-based hole-only devices enhanced with a $CHCl_3$: toluene ratio from 0 : 1 to 1.5 : 1. Furthermore, inkjet-printed TFT based on **3HTBTT** with an optimized solvent system was successfully fabricated and exhibited a hole mobility

of 0.01 $cm^2 V^{-1} s^{-1}$. Optimizing the device structure is expected to further enhance the mobility of inkjet-printed TFTs with **3HTBTT** in the future. Although the performance of this **3HTBTT**-based inkjet-printed TFT was not high as our expectation, our work regarding morphology and crystallinity of newly designed organic semiconductors with the controlling solvent system can serve as a new avenue for optoelectronic applications.

Author contributions

C. K. Trinh: conceptualization, methodology, investigation, visualization, writing – original draft, review & editing, resources. H. S. Oh: investigation. H. Lee: methodology, investigation, writing – original draft, review & editing, resources.

Conflicts of interest

There are no conflicts to declare.

Acknowledgements

We would like to thank Van Lang University, Vietnam for the support of this research. This work was supported by the 2021 Research Fund of Myongji University.

Notes and references

1 Z. Zhan, J. An, Y. Wei, V. T. Tran and H. Du, *Nanoscale*, 2017, **9**, 965–993.
2 Y. Fang, X. Wu, S. Lan, J. Zhong, D. Sun, H. Chen and T. Guo, *ACS Appl. Mater. Interfaces*, 2018, **10**, 30587–30595.
3 P. F. Moonen, I. Yakimets and J. Huskens, *Adv. Mater.*, 2012, **24**, 5526–5541.
4 L. Feng, C. Jiang, H. Ma, X. Guo and A. Nathan, *Org. Electron.*, 2016, **38**, 186–192.
5 B. Kang, W. H. Lee and K. Cho, *ACS Appl. Mater. Interfaces*, 2013, 2302–2315.
6 L. Zhou, L. Yang, M. Yu, Y. Jiang, C.-F. Liu, W.-Y. Lai and W. Huang, *ACS Appl. Mater. Interfaces*, 2017, **9**, 40533–40540.
7 J. Zhao, L.-W. Lo, H. Wan, P. Mao, Z. Yu and C. Wang, *Adv. Mater.*, 2021, **33**, 2102095.
8 X. Chen, R. Huang, Y. Han, W. Zha, J. Fang, J. Lin, Q. Luo, Z. Chen and C. -Q. Ma, *Adv. Energy Mater.*, 2022, **12**, 2200044.
9 X. Meng, Z. Xing, X. Hu and Y. Chen, *Chin. J. Polym. Sci.*, 2022, **40**, 1522–1566.
10 D. Stuwe, D. Mager, D. Biro and J. G. Korvink, *Adv. Mater.*, 2015, **27**, 599–626.
11 Y. Sun, Y. Zhang, Q. Liang, Y. Zhang, H. Chi, Y. Shi and D. Fang, *RSC Adv.*, 2013, **3**, 11925–11934.
12 C. Bax, R. Bernasconi, F. Massironi, L. Magagnin, F. Grizzi, L. Capelli and G. Taverna, *J. Electrochem. Soc.*, 2021, **168**, 047513.
13 Y. S. Rim, S.-H. Bae, H. Chen, N. De Marco and Y. Yang, *Adv. Mater.*, 2016, **28**, 4415–4440.
14 R. G. Scalisi, M. Paleari, A. Favetto, M. Stoppa, P. Ariano, P. Pandolfi and A. Chiolerio, *Org. Electron.*, 2015, **18**, 89–94.
15 Y. Song and Y.-G. Ha, *Bull. Korean Chem. Soc.*, 2020, **41**, 123–126.
16 M. Gao, L. Li and Y. Song, *J. Mater. Chem. C*, 2017, **5**, 2971–2993.
17 C. S. Buga and J. C. Viana, *Adv. Mater. Technol.*, 2021, **6**(6), 2001016.
18 S. Fu, J. Tao, W. Wu, J. Sun, F. Li, J. Li, Z. Huo, Z. Xia, R. Bao and C. Pan, *Adv. Mater. Technol.*, 2019, 1800703–1800711.
19 T. M. Schmidt, T. T. Larsen-Olsen, J. E. Carle, D. Angmo and F. C. Krebs, *Adv. Energy Mater.*, 2015, **5**, 1500569–1500577.
20 H. Lu, J. Lin, N. Wu, S. Nie, Q. Luo, C.-Q. Ma and Z. Cui, *Appl. Phys. Lett.*, 2015, **106**, 093302–093305.
21 R. Mikkonen, P. Puistola, I. Jönkkäri and M. Mäntysalo, *ACS Appl. Mater. Interfaces*, 2020, **12**(10), 11990–11997.
22 J. Lee, D. H. Kim, J.-Y. Kim, B. Yoo, J. W. Chung, J.-Il. Park, B.-L. Lee, J. Y. Jung, J. S. Park, B. Koo, S. Im, J. W. Kim, B. Song, M.-H. Jung, J. E. Jang, Y. W. Jin and S.-Y. Lee, *Adv. Mater.*, 2013, **25**(41), 5886–5892.
23 L. Mu, M. He, C. Jiang, J. Wang, C. Mai, X. Huang, H. Zheng, J. Wang, X.-H. Zhu and J. Peng, *J. Mater. Chem. C*, 2020, **8**, 6906–6913.
24 H.-S. Liao, Y.-X. Hu, X. Xia, D.-D. Xie, H.-J. Chi, Y. Dong, X.-C. Li, Y.-L. Lv, D.-Y. Zhang and X. Li, *J. Organomet. Chem.*, 2022, **957**, 122157.
25 C. Jin, H. Zeng, F. Zhang, H. Qiu, Z. Yang, M. Mutailipu and S. Pan, *Chem. Mater.*, 2022, **34**, 440–450.
26 K. S. Park, J. J. Kwok, P. Kafle and Y. Diao, *Chem. Mater.*, 2021, **33**, 469–498.
27 F. Liu, J. Zhang, Y. Wang, S. Chen, Z. Zhou, C. Yang, F. Gao and X. Zhu, *ACS Appl. Mater. Interfaces*, 2019, **11**(38), 35193–35200.
28 Q. Zhang, B. Kan, F. Liu, G. Long, X. Wan, X. Chen, Y. Zuo, W. Ni, H. Zhang, M. Li, Z. Hu, Y. Cao, Z. Liang, M. Zhang, T. P. Russell and Y. Chen, *Nat. Photonics*, 2015, **9**, 35–41.
29 J. Zhang, J. Lv, X. Dong, T. Xu, X. Dai, T. Duan, Z. Kan, P. Liu and S. Lu, *J. Mater. Chem. C*, 2020, **8**, 9195–9200.
30 C. K. Trinh, J. W. Choi, W. Kim and J.-S. Lee, *Synth. Met.*, 2019, **256**, 116149–116155.
31 C. K. Trinh, J. W. Choi, K. T. Tran, Z. Ahmad and J.-S. Lee, *RSC Adv.*, 2022, **12**, 26400–26405.
32 C. K. Trinh and N. I. Abdo, *J. Mol. Struct.*, 2022, **1269**, 133764–133771.
33 K.-H. Kim, H. Yu, H. Kang, D. J. Kang, C.-H. Cho, J. H. Oh and B. J. Kim, *J. Mater. Chem. A*, 2013, **1**, 14538–14547.
34 S.-H. Kang, D. Lee, H. Kim, W. Choi, J. Oh, J. H. Oh and C. Yang, *ACS Appl. Mater. Interfaces*, 2021, **13**(44), 52840–52849.
35 C. K. Trinh, H.-J. Lee, J. W. Choi, M. Shaker, W. Kim and J.-S. Lee, *New J. Chem.*, 2018, **42**, 2557–2563.
36 D. K. Sagdullina, I. E. Kuznetsov, A. V. Akkuratov, L. I. Kuznetsova, S. I. Troyanov and P. A. Troshin, *Synth. Met.*, 2019, **250**, 7–11.
37 P. Sonar, E. L. Williams, S. P. Singh and A. Dodabalapur, *J. Mater. Chem.*, 2011, **21**, 10532–10541.
38 A. A. El-Shehawy, N. I. Abdo, A. A. El-Barbary and J.-S. Lee, *Eur. J. Org. Chem.*, 2011, 4841–4852.

39 M. Lada, M. J. Starink, M. Carrasco, L. Chen, P. Miskiewicz, P. Brookes, M. Obarowskac and D. C. Smith, *J. Mater. Chem.*, 2011, **21**, 11232–11238.
40 Z. He, Z. Zhang, K. Asare-Yeboah and S. Bi, *Mater. Adv.*, 2023, **4**, 769–786.
41 Y. Lee, D. Ho, F. Valentini, T. Earmme, A. Marrocchi, L. Vaccaro and C. Kim, *J. Mater. Chem. C*, 2021, **9**, 16506–16515.
42 B. Liu, D. Rocca, H. Yan and D. Pan, *ACS Au*, 2021, **1**(12), 2182–2187.
43 M. Planells, M. Nikolka, M. Hurhangee, P. S. Tuladhar, A. J. P. White, J. R. Durrant, H. Sirringhaus and I. McCullocha, *J. Mater. Chem. C*, 2014, **2**, 8789–8795.
44 R. Ams, N. Trapp, A. Schwab, J. V. Milić and F. Diederich, *Chem.–Eur. J.*, 2019, **25**(1), 323–333.
45 M. Echeverri, C. Ruiz, S. Gámez-Valenzuela, I. Martín, M. C. R. Delgado, E. Gutiérrez-Puebla, M. Á. Monge, L. M. Aguirre-Díaz and B. Gómez-Lor, *J. Am. Chem. Soc.*, 2020, **142**(40), 17147–17155.
46 S. J. Nam, S. J. Jeon, Y. W. Han and D. K. Moon, *J. Ind. Eng. Chem.*, 2018, **63**, 191–200.
47 M. Shaker, J.-H. Lee, C. K. Trinh, W. Kim, K. Lee and J.-S. Lee, *RSC Adv.*, 2015, **5**, 66005–66012.
48 C. K. Trinh, G. M. Nassar, N. I. Abdo, S. Jung, W. Kim, K. Lee and J.-S. Lee, *RSC Adv.*, 2022, **12**, 17682–17688.
49 M. Li, M. Xiao and Z. Li, *RSC Adv.*, 2021, **11**, 39625–39635.
50 C. E. S. Bernardes, M. L. S. M. Lopes, J. R. Ascenso and M. E. M. da Piedade, *Cryst. Growth Des.*, 2014, **14**(11), 5436–5441.